Changes in resonance frequency of rock columns due to thermoelastic effects on a daily scale: observations, modelling and insights to improve monitoring systems

Antoine Guillemot, Laurent Baillet, Eric Larose, Pierre Bottelin

Geophysical Journal International

Geophys. J. Int. (2022) **231,** 894–906
Advance Access publication 2022 June 10
GJI Seismology

https://doi.org/10.1093/gji/ggac216

Changes in resonance frequency of rock columns due to thermoelastic effects on a daily scale: observations, modelling and insights to improve monitoring systems

Antoine Guillemot,[1,2] Laurent Baillet,[1] Eric Larose[1] and Pierre Bottelin[3]

[1]*Laboratoire ISTerre, Université Grenoble Alpes, CNRS, Université Savoie Mont Blanc, 38000 Grenoble, France.*
E-mail: antoine.guillemot@univ-grenoble-alpes.fr
[2]*Géolithe and Géolithe Innov, 38920 Crolles, France*
[3]*Association pour le Développement des Recherches sur les Glissements de terrain (ADRGT); 2 rue de la Condamine BP17 38610 Gières, France*

Accepted 2022 June 7. Received 2022 June 1; in original form 2022 February 10

SUMMARY

Slope instabilities, including prone-to-fall rock columns, are known to exhibit clear vibrational modes. The resonance frequencies of these modes can be tracked by seismic instrumentation, allowing the rock column's mechanical and structural properties to be monitored, as well as providing precursors of imminent irreversible failures. In previous studies, superficial thermoelastic effects were assumed to drive daily fluctuations in resonance frequencies, but no qualitative or quantitative evidence was provided. The results presented here corroborate this hypothesis and quantify the physical processes involved. We interpreted daily variations of resonance frequencies in the Les Arches study site (Vercors, French Prealps) using a thermo-mechanical finite-element model. Modelled fluctuations of the resonance frequencies over a day closely matched experimental observations, reproducing the daytime frequency increase of around 2 per cent. In addition, our model provides explanation of the various behaviours observed across study sites: the frequency response strongly depends on solar exposure, as well as the timing and intensity of both radiative and convective heat fluxes. We highlight acousto-elastic constants as key parameters of our semi-quantitative model, although they remain poorly constrained here. For future instrumentation, we therefore recommend the deployment of pyranometers on rocky sites to accurately invert these parameters over time, thus allowing rock fracturing to be quantitatively tracked by acousto-elastic monitoring.

Key words: Fourier analysis; Numerical modelling; Acoustic properties; Seismic noise.

Introduction

Since unstable rock sites may be the cause of significant geohazards in mountainous regions, critical sites are most often instrumented to predict catastrophic events and mitigate any damage downslope (Colombero *et al.* 2021a). Over the last few decades, there has been a growing interest in environmental seismology as a means to monitor changes in the Earth's subsurface. In a transdisciplinary context, this research field combines fundamental studies, natural hazard assessment, and risk management (Larose *et al.* 2015). Long-term seismic monitoring systems provide a set of methods to characterize and monitor the volume of slope instabilities, including landslides and potentially unstable rock sites as rockslides and rock columns. These systems generally involve continuous recording of ambient noise by passive seismometers. Several observables can be extracted from these seismic data: (i) relative seismic velocity changes (often called dV/V) retrieved from ambient noise cross-correlations, and (ii) modal parameters such as resonance frequencies (f_i), modal shapes and attenuation retrieved from spectral analysis of ambient noise recordings (Burjánek et al. 2010; C. Colombero *et al.*2015, 2016; Larose et al. 2015; Häusler *et al.* 2019; Dietze *et al.* 2020). Both dV/V and modal parameters are directly related to the geometry and elastic behaviour of the medium monitored, such as its stiffness and its density. Seismological monitoring methods are thus useful to investigate and keep track of the mechanical state of potentially unstable sites. Several studies have shown the applicability of these methods to track the failure of rock columns (Levy et al. 2011; P. Bottelin *et al.* 2017; Colombero *et al*. 2021b; Pierre Bottelin *et al*. 2021), jointed rock masses (Grechi & Martino 2021), slope instabilities (Iannucci *et al.* 2018; Dietze *et al.* 2020) and the acceleration of clayey landslides (Mainsant *et al.* 2012; Bièvre *et al.* 2018; Fiolleau *et al.* 2020).

From these studies, it has emerged that temperature variations, precipitations, freezing and changes in atmospheric pressure are the major environmental factors triggering reversible changes in the mechanical parameters of rocks. For monitoring purposes, these

reversible effects must be distinguished from irreversible changes due to physical processes which could potentially lead to failure (fluidization for landslides; crack formation, alteration and destabilization for rock instabilities). Although the interpretation of changes in seismological observables is often not straightforward (see reviews from Le Breton *et al.* 2021; Colombero *et al.* 2021a), there remains a need for a comprehensive understanding and a quantitative assessment of the respective effects of the environmental forcings exerted at rock sites. Among the environmental drivers identified, thermal effects are particularly relevant in rock walls and rock columns (Vlcko et al. 2009; do Amaral Vargas et al. 2013; Gischig *et al.* 2015; Collins & Stock 2016; Draebing *et al.* 2017; Leith *et al.* 2017; Collins *et al.* 2018; Villarraga *et al.* 2018). Surface rock temperature can be directly measured using thermal cameras and thermistors, yielding valuable—albeit superficial—information. In summer in a temperate climate, sun-exposed rock surface temperatures can undergo considerable changes over the course of a day, with amplitudes of about 20 K (Guerin *et al.* 2019; Racek *et al.* 2021a). Significant variations in energy fluxes can also accumulate within the rocky mass as a result of these daily changes, or due to seasonal fluctuations in air temperature and sun exposure (Grechi et al. 2021). However, the temperature field inside the rock mass remains poorly known, as temperature and solar radiation are generally measured on the surface. Few studies have quantified solar radiation (also called radiative heat flux) in the field using pyranometers (Racek *et al.* 2021b). Nevertheless, radiative heat flux is known to be strongly influenced by the orientation of the slope and its exposure to the sun, with a maximum value of about 1000 W m^{-2} (Racek *et al.* 2021a).

Significant thermal forcing at the surface leads to diffusion of a heat wave in the rock body, modifying its stress state, thus changing its mechanical behaviour (Marmoni et al. 2020). Seismological observables, such as seismic velocities and resonance frequencies f_i, may reflect these thermally induced processes. Many field-studies report correlations between temperature of the air T_a and resonance frequencies f_i with various temporal scale, amplitude and delay time.

Most of the studies report a positive T_a-f_i correlation at daily scale (P. Bottelin *et al.* 2013, 2017; Starr *et al.* 2015; C. Colombero *et al.* 2017, 2018; J. Valentin *et al.* 2017; Burjánek *et al.* 2018; J. Valentin 2018, see Colombero *et al.* 2021a, for review). When quantified, the daily relative variation in resonance frequencies ($\Delta f_i / f_i$) ranges between 1.5 and 6.5 per cent. The time delay between changes in air temperature and altered resonance frequency is highly variable, generally ranging between 0 and 4 hr (Colombero *et al.* 2021a). On a daily scale, the periodic thermal wave front does not penetrate the rock more than a few centimetres: thermal forcing therefore remains superficial. Rock expansion in this shallow layer may partly close the rear fracture (RF) and increase contact stiffness between the stable cliff and the column (P. Bottelin *et al.* 2013). Alternatively (or in complement), superficial rock expansion induces differential stress, thus generating a confining pressure which increases the effective elastic moduli of the rock column (Larose & Hall 2009; Tsai 2011; Richter *et al.* 2014; Starr *et al.* 2015). This process yields an increase in both seismic relative velocity ($dV/V > 0$) and the resonance frequencies f_i measured on the rock column.

A negative T_a-f_i correlation is rarely observed when monitoring seasonal fluctuations. At a seasonal scale, this negative correlation may be interpreted as a bulk thermal effect on elastic properties: the whole column is affected by the seasonal change in the rock's temperature T. An increase in T may lead to a decrease in the effective elastic moduli of the volume (Xia *et al.* 2011), but this effect is tiny and mostly overwhelmed by thermo-mechanical strain stiffening. These negative correlation is rather linked to site-specific RF geometry effects, or freezing (Colombero *et al.* 2021a).

In this paper, we delve further into the interpretation of the positive correlation between air temperature and resonance frequencies at daily scale. Since resonance frequency tracking is the most direct way to observe and model thermo-mechanical issues on rock columns, rather than dV/V monitoring, we focused on resonance frequency results in this paper. First, we propose a semi-quantitative assessment of thermally induced stresses within a rock column, providing details of theoretical and experimental studies of acousto-elasticity. Then, we reinterpret seismic observations recorded on an unstable limestone column at the Les Arches site (Vercors, French Alps). For this purpose, we developed and executed a finite-element thermo-mechanical model which considers acousto-elastic effects. We then discuss the results and limitations of our model. We finally underline the benefits of taking thermo-acoustoelastic effects into account for monitoring purposes, and propose adaptations in terms of instrumentation strategies and slope-instability modelling.

Study site description

For this study, we focused on the prone-to-fall rock column at Les Arches (Vercors, French Prealps, see full description in P. Bottelin *et al.* 2013). The site's location and a picture of the column are shown in Figs 1(a) and (b), respectively. The rock cliff is composed of fractured, highly porous bioclastic limestone (known as Glandasse limestone). The first three experimental resonance frequencies of the column (labelled f_{1e}, f_{2e} and f_{3e}, respectively) were picked out on passive seismic recordings. Their average values over the course of summer 2009 were 6.0, 6.9 and 8.8 Hz, respectively. Winter and freezing temperatures caused fluctuations in f_i and/or unclear resonance values to emerge, and were therefore not processed in this paper. Meteorological data were continuously recorded at a station located 3 km from the site at an altitude 120 m lower. Over summer 2011, filtered time-series showed a clear positive correlation between the fundamental frequency f_{1e} and air temperature T_a at a daily scale. Thus, the air temperature T_a oscillated between 283 and 298 K. Relative change in frequency amplitude response was about ±2 per cent and followed after a 4.5-hr delay (see full description in P. Bottelin *et al.* 2013 and Fig. 2). On this site, thermal forcing was not directly measured, we thus lack strong quantification of the heat fluxes.

Acousto-elasticity theory

Various environmental phenomena can cause variations in elastic wave velocity, including air and rock temperature, water content, freeze-thawing cycles and chemical variations (Larose & Hall 2009; Le Breton *et al.* 2021). For this study, we focused on the influence of temperature of the medium, since it clearly acts as the major driving parameter during the daytime in summer (Colombero *et al.* 2021a).

A direct link has been established between the temperature of an elastic material T and its mechanical wave velocity: when T increases, micro-cracks dilate and the free structure as a whole expands, leading to a decrease in wave velocity. This effect has been observed notably for multiple scattered acoustic coda waves in homogeneous concrete structures (Larose *et al.* 2006). As an example, coda wave interferometry revealed a thermal dilation rate of acoustic velocities in concrete of 0.15 per cent K^{-1}, suggesting

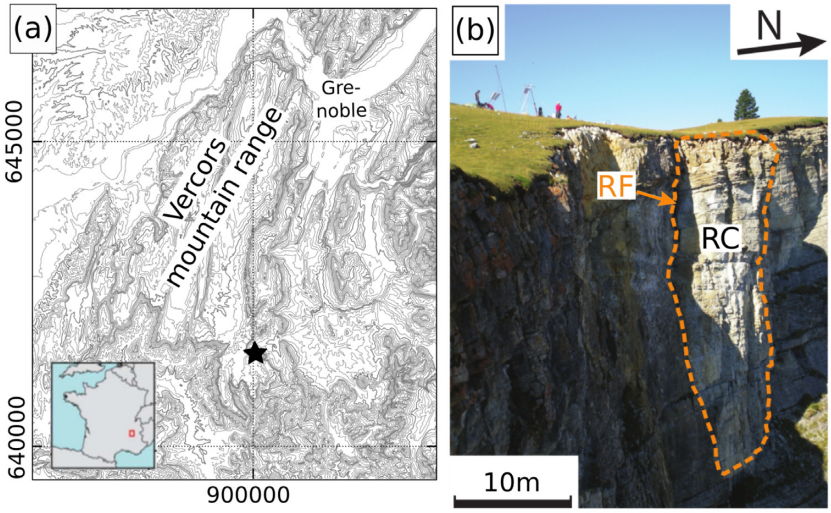

Figure 1. (a) Map showing the location of the study site. The 'Les Arches' site is indicated by the black star. Coordinates are given in Lambert 93 (EPSG2154). (b) Picture of the prone-to-fall rock column (RC) taken from south-east into north-west direction. The RF is delineated by the orange dashed line.

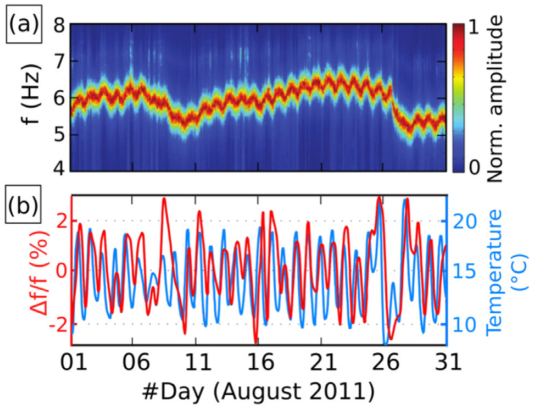

Figure 2. (a) Monitoring of the fundamental frequency f_{1e} for Les Arches site throughout 2011 August. The colour scales with spectrum amplitude were normalized between 0 and 1. (b) Relative variation of the fundamental frequency f_{1e} ($\Delta f_{1e}/f_{1e}$) at daily scale over the same period (red continuous line). Daily changes in air temperature are indicated by the continuous blue line. Data and results are adapted from P. Bottelin *et al.* (2013).

that this was an accurate method to monitor this thermal effect in a damage-assessment context. Nevertheless, the negative correlation between temperature of the medium T and acoustic wave velocity cannot explain the positive correlation observed between T and resonance frequency in most studies, since elastic (or acoustic) wave velocities and resonance frequencies are positively correlated and directly linked.

Another effect must therefore be taken into account: for a confined structure subjected to heat fluxes at its surface, a confinement pressure occurs as a result of differential dilation inside the structure, described as additional thermally induced stress. Such changes in mechanical strain or stress field cause variations of wave velocity propagating through the medium. This relation forms the basis of acousto-elasticity, which has been extensively described both theoretically and experimentally (Murnaghan 1951; Bach & Askegaard 1979; Larose & Hall 2009; Tsai 2011; Xie *et al.* 2018). For most materials, additional stress causes higher rigidity leading to an increase in wave velocity (Planès & Larose 2013). The influence of solar heat flux on the Earth's subsurface elasticity has also been revealed thanks to geodesic measurements, along with stress and seismic velocity monitoring (Tsai 2011; Richter *et al.* 2014). These observations can be modelled based on thermally induced stresses (Tsai 2011). At a smaller scale, the positive correlation found between air temperature and resonance frequency (or seismic velocity) in Les Arches (P. Bottelin *et al.* 2013) could also be effectively explained by thermo-acousto-elasticity.

Consequently, we applied the acousto-elasticity equations presented by Murnaghan (1951) to the Les Arches rock column presented in Fig. 1. To quantify this relation in a simple case, we considered a normal (uniaxial) stress σ applied to a uniform solid medium with a body wave velocity V_{ij}^0 propagating in direction i and polarized in direction j. An additional stress $\Delta\sigma$ (e.g. thermally induced) is then applied, leading to a modification of the wave velocity in the first order, as described below:

$$Vi_j = V_{ij}^0 + \frac{\partial V_{ij}}{\partial \sigma}\Delta\sigma \tag{1}$$

where $o(\in)$ is negligible that

Introducing the relative velocity change, this relation becomes:

$$\frac{V_{ij} - V_{ij}^0}{V_{ij}^0} = A_{ij}\Delta\sigma \tag{2}$$

This formalized relation introduces an acousto-elastic constant A_{ij}, which can be expressed as:

$$\langle A_{ij}\rangle = -\frac{\beta}{E} \tag{3}$$

E is the Young modulus of the material, whereas the coefficient $\beta < 0$ is strongly related to its second (Lamé) and third (Murnaghan) elastic constants (Tsai 2011; Planès & Larose 2013; Richter *et al.* 2014).

We account for the acousto-elastic effect by the relation between hydrostatic pressure (or stress) and elastic P and S waves. We average eq. (2) in all directions, assuming that thermal stress applied to a rock column acts like an isotropic confining pressure. The relative velocity change then becomes linear with the absolute stress variation, as described by eqs (4a) and (4b) below:

$$V_P = V_P^0\,(1 + A_P\Delta\sigma) \tag{4a}$$

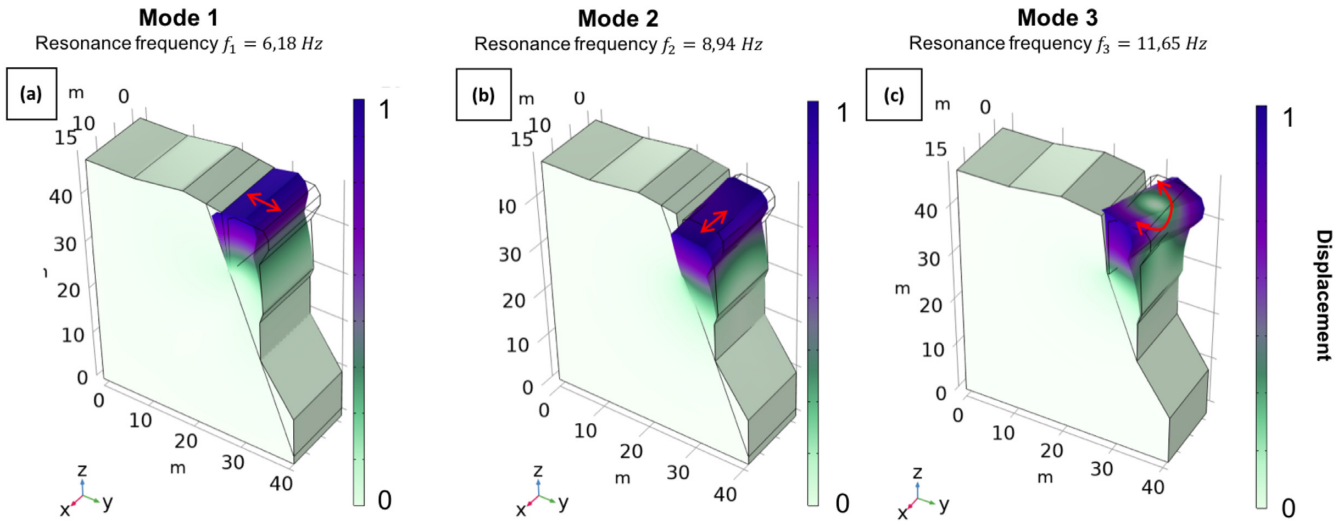

Figure 3. (a)–(c) 3-D visualization of the first three vibration modes of the modelled rock column at Les Arches. Colour indicates the normalized displacement amplitude of the column. The red arrow indicates the main direction of vibration.

$$V_S = V_S^0\ (1 + A_S \Delta\sigma) \tag{4b}$$

with the usual definition of *P*- and *S*-wave velocities:

$$V_P^0 = \sqrt{\frac{E\,(1-\upsilon)}{(1+\upsilon)(1-2\upsilon)\,\rho}} \tag{5}$$

$$V_S^0 = \sqrt{\frac{E}{2\,(1+\upsilon)\,\rho}} \tag{6}$$

Several studies have reported highly variable experimental values of parameters A_i for various rock materials (Murnaghan 1951; Hughes & Kelly 1953; Johnson *et al.* 1999; Guyer & Johnson 2009; Richter *et al.* 2014). Moreover, it is worth noting that this acousto-elastic constant is very sensitive to aging and the degree of rock mass fracturing (Planès & Larose 2013). Hence, the acousto-elastic constant for a highly damaged (altered) material is generally one order of magnitude higher than that of the corresponding healthy material, making a precise estimation of its value difficult without recourse to damage-assessment of rock samples. This statement will be discussed in the following section, where we deal with modelling issues as well as monitoring damage and fracturing.

Thermo-mechanical modelling

We simulated the behaviour of the Les Arches rock column using both modal analysis and a transient thermo-mechanical analysis (TTMA). To do so, we built a 3-D finite-element model using the *COMSOL Multiphysics* software 2022, applying a simple geometry constrained by a Digital Elevation Model derived from Lidar measurements. The column is 30 m high, 15 m wide and 5 m thick at its top. The open RF (see Fig. 1b) separates the column from the stable cliff, extending to 15 m depth. Our model was composed of 25 000 quadratic tetrahedral finite elements, with maximum size of 0,9 m side. To adequately resolve surficial changes in the rock mass, we added 10 boundary layers to the mesh in order to densify the elements located near the surface of the 3-D rock column. Elements from boundary layers form a smooth transition to interior mesh, with averaged size of 0,05 m side. This mesh refinement provided a precision better than 1 per cent in all computed thermo-mechanical fields over the range of frequencies below 50 Hz. The fractured limestone composing the rock column was modelled by a homogeneous linear elastic material, with Young modulus $E = 6900$ MPa, Poisson's ratio $\nu = 0.43$ and density $\rho = 2650\ \mathrm{kg\,m^{-3}}$ (Lévy *et al.* 2010; P. Bottelin *et al.* 2013).

Modal analysis yielded numerical resonance frequencies for the structure (f_{in}), as well as associated modal shapes. The first three vibration frequencies f_{1n}, f_{2n} and f_{3n} were 6.2, 8.8 and 11.6 Hz (Fig. 3), close to the experimental values (f_{1e} 6.0 Hz, f_{2e} 7.5 Hz and f_{3e} 9.0 Hz). As expected, the first (respectively, the second) mode corresponds to flexure of the rock column in the direction perpendicular (respectively, parallel) to the RF, whereas the third mode reflects torsion around the vertical axis.

To perform TTMA, we simulated heat fluxes to reproduce realistic daily thermal forcing. Four heat fluxes evolving over time were imposed on the geometry, and are summarized in Fig. 4:

i) a convective heat flux Q_{conv} based on the temperature of the air T_a in direct contact with the rock wall. This convection was applied to the top of the cliff and to the surface of the rock column, with a heat transfer coefficient $h_1 = 50\ \mathrm{W\,m^{-2}\,K^{-1}}$, as described below:

$$T_a = T_0 + \Delta T \sin\left[2\pi f\,(t - \varphi_{\mathrm{conv}})\right] \tag{7}$$

$$Q_{\mathrm{conv}} = h\,(T_{\mathrm{ext}} - T) \tag{8}$$

This expression reflects the thermal forcing induced by the air temperature at a daily scale, with the daily mean air temperature $T_0 = 20\,^{\circ}\mathrm{C}$, the daily amplitude of the sinusoidal oscillation $\Delta T = 10\,^{\circ}\mathrm{C}$, the periodicity $f = 1\ \mathrm{day^{-1}}$ and the phase $\varphi_{\mathrm{conv}} = 10:00$ AM.

i) a convective heat flux similar to (i) but located only inside the RF of the column. The parameter that distinguishes this flux from (i) is the thermal exchange coefficient, which was taken at a much lower value due to the sheltering effect inside the fracture. We set this coefficient at half an order of magnitude lower than the first $h_2 = 10\ \mathrm{W\,m^{-2}\,K^{-1}}$. The value applied to this coefficient is very approximate, but was shown to play only a minor role in the subsequent study.

ii) a radiative heat flux Q_{rad} based on the solar radiation hitting the external surface of the rock column. Assuming similar solar

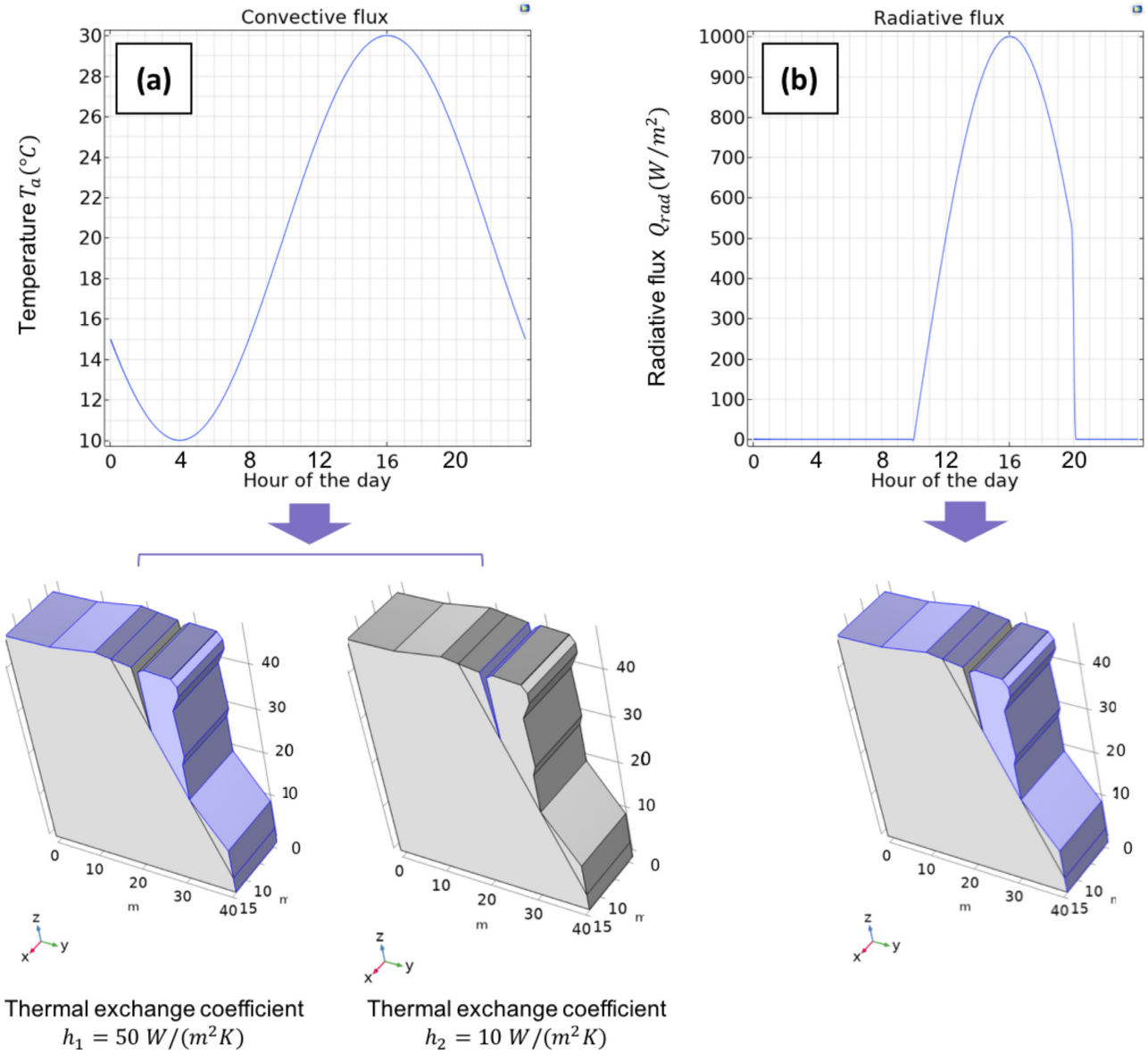

Figure 4. Daily thermal forcing imposed on the surface of the 3-D geometry. Top (a) air temperature T_a over time used as input to model convective heat flux. (b) Radiation over time used as input to model radiative heat flux Q_{rad}. Bottom Heat flux applied to surfaces with the geometry shown, highlighted in blue.

conditions to those described by Racek *et al.* (2021a), we modelled this flux as a smoothed periodic impulse acting once a day, with a maximum value $q_{\max} = 1000\ \text{W m}^{-2}$ and lasting 10 hr per day. For the sake of simplicity, we made the strong assumption that the maximum values of radiative and convective fluxes were synchronized (at 4:00 PM). In reality, convective and radiative heat fluxes may not be in phase. We later address the effect of time shifts in fluxes in the discussion section and Appendix B.

iii) A geothermal heat flux located at depth within the structure (more than 20 m), usually fixed at the constant value $q_{\text{geo}} = 5 \times 10^{-2}\ \text{W m}^{-2}$. But as expected for a daily-scale study, we confirmed that this flux had a negligible influence on results compared to those of the other surface fluxes mentioned above.

The thermal fluxes (i)–(iii) applied to the surface led to changes in the temperature field inside the rock column, as a result of heat diffusion. Heat wave propagation was modelled by applying the usual Fourier heat diffusion equation, assuming a thermal conductivity of limestone of the order of $k = 1\ \text{W m}^{-1}\,\text{K}^{-1}$ and a thermal capacity at constant pressure of $C_p = 800\ \text{J kg}^{-1}\,\text{K}^{-1}$ (P. Bottelin *et al.* 2013; Lowrie & Fichtner 2020).

Fluctuations to the rock temperature field cause a change in stress conditions within the rock column as a result of thermally induced expansion. The thermal expansion coefficient for the whole rock structure was fixed at $\alpha = 2,8 \times 10^{-6}\,\text{K}^{-1}$ (Feng *et al.* 2020).

The acousto-elastic constant $A_{P,S}$ was evaluated using the range of $\partial\rho V^2/\partial\sigma$ values reported (Winkler & McGowan 2004; Richter 2014), and applying the following relation:

$$A_j = b_j \frac{(1-\nu)}{E} \frac{\partial \rho V_j^2}{\partial \sigma} \tag{9}$$

With

$$b_P = \frac{(1+\nu)(1-2\nu)}{2(1-\nu)^2} \sim 0.3 \text{ for } P\text{–waves} \tag{10a}$$

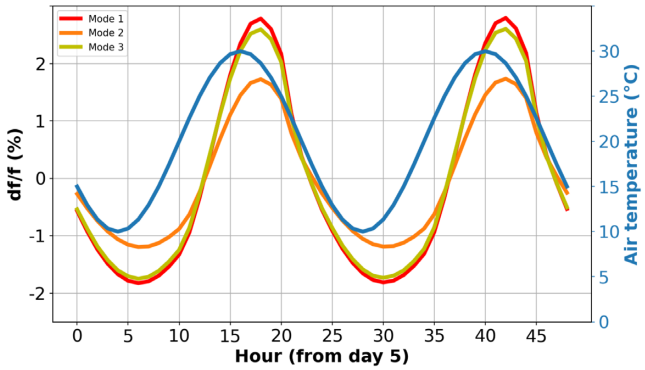

Figure 5. Relative change over time of resonance frequency of the first three modes for the modelled rock column at Les Arches $\Delta f_i/f_i$ (fundamental mode $i = 1$ in red, mode $i = 2$ in orange and mode $i = 3$ in yellow), along with the air temperature imposed T_a (in blue). Only two days at steady state (days 5 and 6) of the transient simulation TTMA are shown.

$$b_S = \frac{1+\nu}{1-\nu} \sim 2.5 \text{ for } S\text{–waves} \tag{10b}$$

Eq. (9) yields $A_P \in [2 \times 10^{-8}; 6 \times 10^{-8}]\text{Pa}^{-1}$ and $A_S \in [1 \times 10^{-7}; 5 \times 10^{-7}]\text{Pa}^{-1}$ for healthy limestone samples at laboratory scale. According to the increase of this value by around one order of magnitude for fractured and altered material (Planès & Larose 2013) and assuming a high degree of fracturing and porosity for the rock column (see Part 2 and Fig. 1b), we set the acousto-elastic constants to $A_P = 6 \times 10^{-8}$ Pa^{-1} and $A_S = 5 \times 10^{-7}$ Pa^{-1}.

We applied the TTMA to the rock column with a temporal step of 1 hr. The simulation duration was set to 6 d. It showed a permanent regime for the variable fields (temperature and stresses) over the last 4 d. We estimated the resonance frequency of the structure by computing a modal analysis, with temperature, stress and elastic fields monitored hourly throughout the permanent regime. The change over time to the RF gap was also estimated by our TTMA: it corresponds to the relative displacement between the rock column and the stable part of the cliff. Fracture opening corresponds to a positive displacement, whereas fracture closing corresponds to a negative displacement. To distinguish the influence of convective heat flux from that of radiative flux, we also ran the same simulation by imposing only the convective heat flux. In complement to these results, changes to pressure, temperature and displacement on the rock column over time were evaluated for each simulation.

Thermo-mechanical results

The relative variations in numerical resonance frequencies f_{1n}, f_{2n} and f_{3n} in response to both convective and radiative thermal forcing are shown in Fig. 5. Our results show good agreement between numerical frequency variations and air temperature T_a: the fundamental frequency correlates positively with T, and the amplitude $\Delta f_i/f_i$ (around ±2.5 per cent) and time delay (around 2.5 hr) are close to experimental observations (Fig. 1b, Bottelin *et al.* 2013).

Temperature, pressure, *P*- and *S*-wave velocity fields inside the rock body are presented at four times during the day (Fig. 6 and Appendix A).

RF opening is observed to negatively correlate with and follow the same sinusoidal pattern as air temperature when considered at a daily scale (Fig. 7). A detectable time delay of about 2.5 hr is observed, almost in phase-opposition with the resonance frequencies recorded (see Fig. 7d). The amplitude of RF gap variations over a day is around 2 mm (Fig. 7b), according to several studies (see Colombero *et al.* 2021a).

Discussion

The aim of this study was to model the effects of thermal forcing and its relation to resonance frequency on a prone-to-fall rock column. Our TTMA analysis revealed physical relations between thermal forcing acting on the rock column and resonance frequency at a daily scale. During daytime, convection warms up the rock surface and solar exposure adds a positive radiative heat flux. Heat penetrates the rock body until 1 m depth by diffusion, inducing a differential expansion within the rock mass at depth during daytime (Fig. 6). This generates thermally induced stresses in the bulk rock, leading to an increase of elastic parameters and wave velocities (+3 per cent for *P*-wave velocity, +19 per cent for *S*-wave velocity at the near-surface, see Fig. A1 in Appendix A). This change in stress field penetrates until around 50 cm inside the rock column drives changes in resonance frequencies at a daily scale. In response, the resonance frequencies increase by several percent. At nighttime, when radiative flux disappears and convective flux cools the rock surface, the resonance frequency decreases, returning to its original value (Fig. 5). These frequency oscillations show a stable permanent regime which has been measured in the field and is reported elsewhere (Colombero *et al.* 2021a). The amplitude and delay response modelled by TTMA compare very well to values measured at the Les Arches site (Bottelin *et al.* 2013).

For the fundamental mode, the amplitude of the decrease in resonance frequency at night is lower (around −1.5 per cent) than the corresponding increase during daytime (+2.5 per cent, Fig. 5). In contrast, the experimental positive and negative variations were of the same order of magnitude (Bottelin *et al.* 2013). This discrepancy may be due to the lack of consideration of the outgoing radiative emission (assimilated to black body radiation) occurring at nighttime on the surface of the rock column. This negative energy flux is not taken into account in our model, even though it should significantly cool the rock mass during the night. This would lead to a more significant drop in frequency in the absence of positive radiative flux.

For all three modes modelled, the respective variations in resonance frequencies show the same sinusoidal pattern, with comparable orders of magnitude (±2 per cent) over time (Fig. 5, red, orange and yellow curves). However, the amplitude variation for fundamental mode f_{1n} is higher than for modes f_{2n} and f_{3n}, suggesting a higher sensitivity to daily thermal cycles. More precisely, the frequency of the second mode is less sensitive to thermal effects than the first and third modes (Fig. 5, yellow curve). For the thermal conditions applied, this difference in sensitivity can be related to the geometry of the rock column, together with the corresponding modal shape (global solicitation as bending or torsion).

We assessed the respective influence of convective and radiative heat fluxes on resonance frequency. Hence, our simulations reveal that around 50 per cent of relative frequency variations are due to convective heat flux induced by air temperature (see Appendix C), whereas the rest is due to the influence of solar radiation. The respective significance of these factors should be quantitatively investigated in future studies, using time-series from pyranometers and thermistors installed on sites. In particular, such studies may better explain the variability of $\Delta f_i/f_i$ amplitude over time by meteorological conditions.

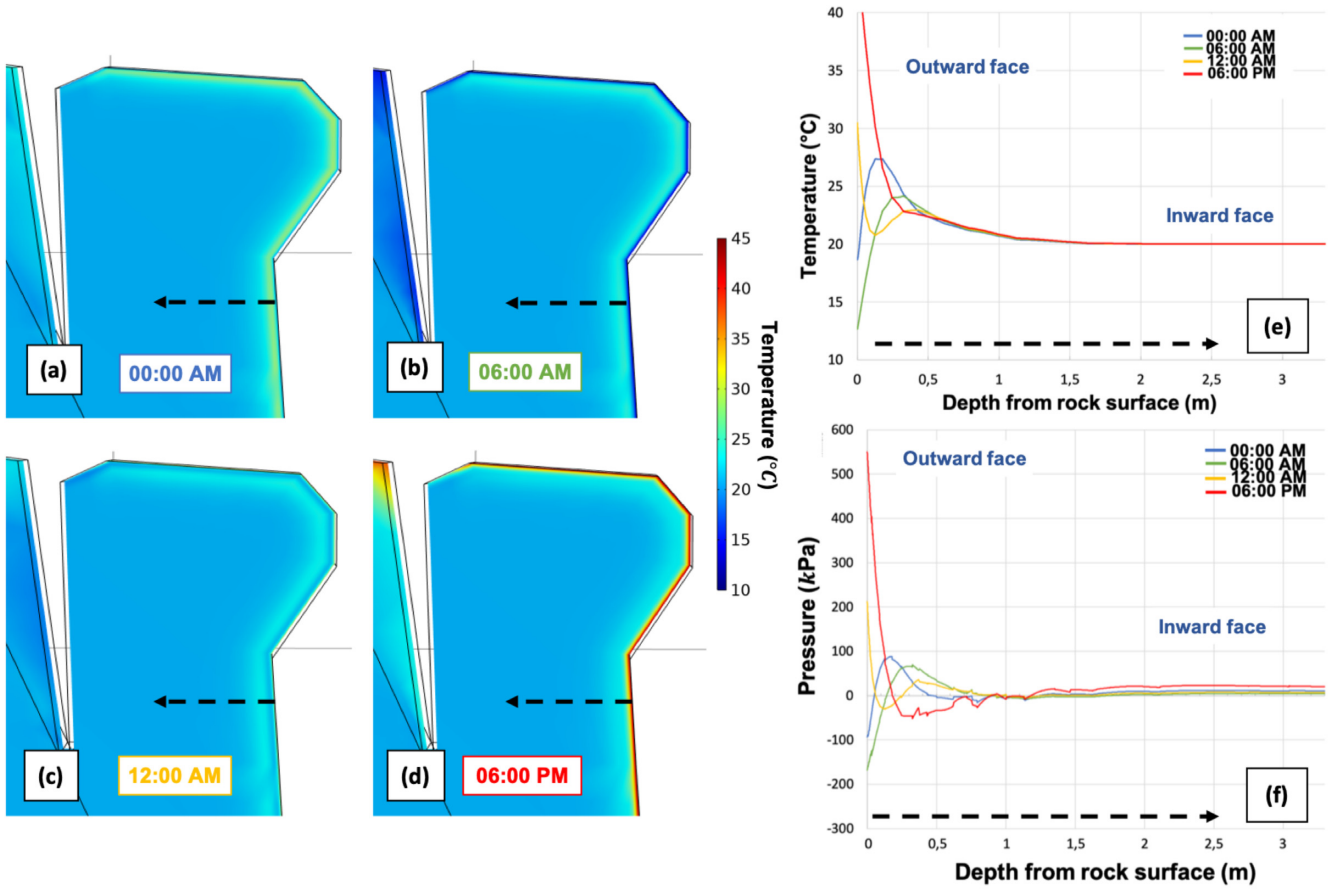

Figure 6. Evolution of the temperature field over time on a vertical cross-section inside the rock model, at scheduled time intervals on day 6 of simulation: (a) midnight, (b) 06:00 AM, (c) midday and (d) 06:00 PM. (e) Temperature and (f) pressure profiles along the modelled rock column (highlighted by the dashed black arrow on cross-sections) are also shown at these four times (colour code indicated in the legend).

In addition, we noted that the time delay between the modal response and thermal forcing is strongly linked to the timing and duration of convective and radiative heat fluxes during the day. In our model, we made the strong assumption that both fluxes have a simultaneous maximum (reached at around 4:00 PM). In reality, convective and radiative heat fluxes may not be in phase. Indeed, exposure of the column to sun is really more complex that the singular, external face exposure simulated in our model. We hypothesize that the time delay measured between the air temperature T_a and the resonance frequencies f_{in} is controlled by (i) differences in the timing of heat fluxes, and (ii) variability in the orientation of the rock column with respect to the sun. To illustrate this hypothesis, we simulated a radiative flux shifted two hours earlier than the convective flux (see Appendix B). As expected, the time delay observed with the fundamental frequency f_{1n} shifted one hour earlier compared to the simulation with simultaneous heat fluxes (Fig. B1). Once again, future field instrumentation with pyranometers and thermistors installed at several locations, in multiple geometries and orientations should improve our understanding of the amplitude of the frequency response, as well as the variability of its delay time across the sites studied (Colombero *et al*. 2021a).

The amplitude of the relative change in resonance frequency $\Delta f_i / f_i$ is mainly controlled by a small number of parameters acting on our thermo-acousto-model. The thermal dilation coefficient, thermal diffusivity and elastic parameters appear confidently constrained for our case study. In contrast, we roughly assessed the acousto-elastic constants A_P and A_s with some uncertainties. These uncertainties are related to our poor knowledge of the degree of fracturing, mesoscopic damage and porosity of the material composing the rock column. Our results show that these acousto-elastic constants are key parameters that characterize resonance frequencies measured on unstable rock masses in response to thermal forcing at a daily scale. The larger the acousto-elastic constants, the larger the daily amplitude of the change in resonance frequencies. Study of this parameter in the field may also reveal the state of fracturing and damage of the material on site.

In addition to these results on resonance frequency, our numerical model also performed very well in simulating the daily cycle of opening and closing of the RF induced by thermal dilatation (Fig. 7). Both the magnitude and time delay are comparable to those reported following experimental observations (Starr *et al.* 2015; Valentin *et al.* 2017; Burjánek *et al.* 2018; Colombero *et al.* 2018). We interpret the negative correlation with rock surface temperature T as a consequence of the thermal expansion of the rock column upon warming, which closes the RF. In addition, according to the model, fracture opening correlates negatively and almost in phase with oscillations of fundamental frequency f_{1n} (Fig. 7d). The increase in frequency is almost in phase-opposition with displacement, with just a slight delay (less than 10 min) with respect to closure of the fracture (Fig. 7d). This offset between fracture displacement and resonance frequencies is modified if convective and radiative fluxes are not synchronized (see Appendix B) or if only the convective flux

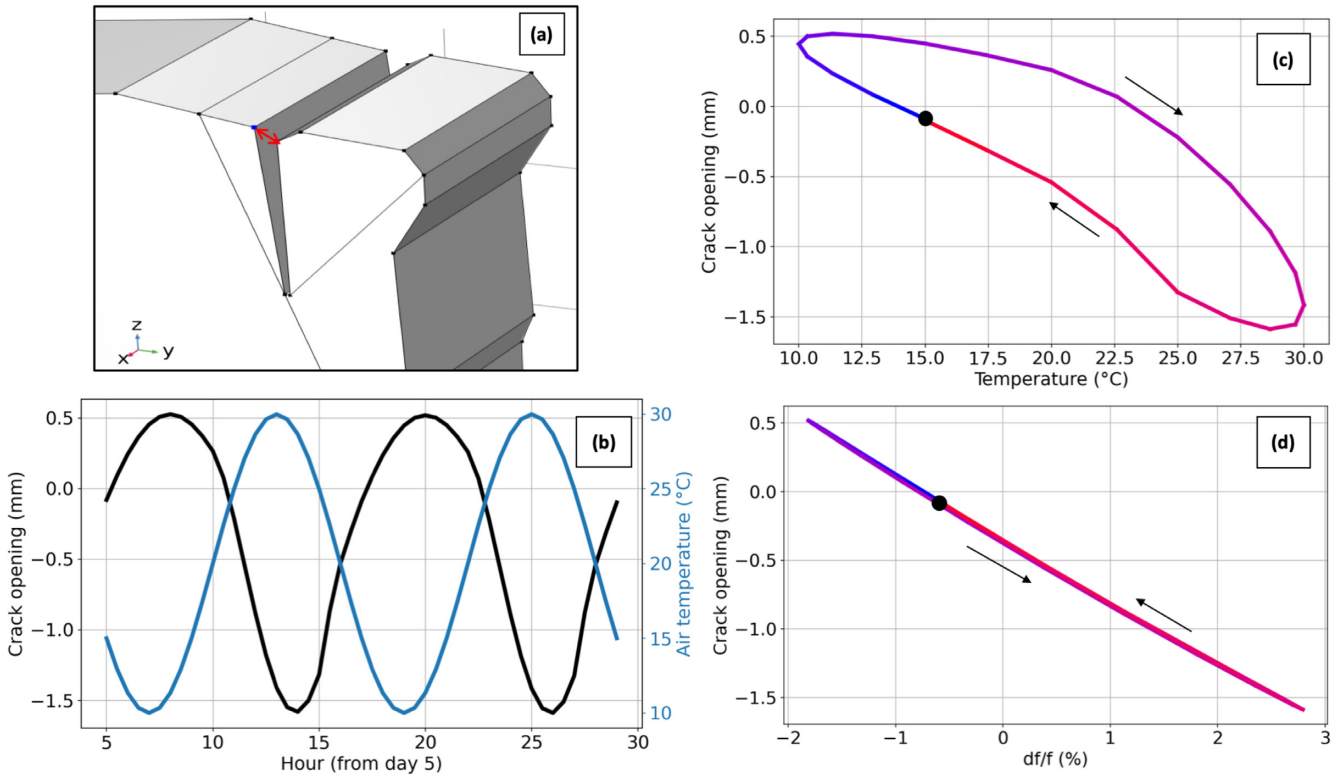

Figure 7. (a) Crack displacement is defined as the gap between the two points on either side of the RF, as indicated by the red arrow. (b) Change to the air temperature (in blue) and crack opening (in black) over time over the course of two days at steady state. (c) Fluctuations of crack opening with respect to the air temperature, over one day in steady state. (d) Fluctuations of crack opening with respect to the relative variation of the fundamental resonance frequency, over one day at steady state. For (c) and (d), temporal evolution is indicated by the line colour, from blue at the beginning (00:00 AM) to red at the end of the day (11:59 PM).

is applied (see Appendix C). This dependency of our results on the timing and intensity of heat fluxes could explain the high variability of observations between sites. It also reinforces the need to fit rock columns with pyranometers to allow quantitative interpretation of changes in resonance frequencies at daily scale.

Conclusion

As a semi-quantitative proof of concept, the thermo-mechanical model using acousto-elasticity presented here supports our assumption about the influence of daily temperature variations on the modal parameters of unstable rock structures, and confirms the impact of thermally induced stress. We recommend further field experiments with specific instrumentation on rocky sites, with the goal of obtaining simultaneous measurements of surface temperature by thermistors, solar radiation by pyranometers, fracture opening by extensometers and resonance frequencies by seismometers. Using these data, it may be possible to calibrate the model on a reference deformation, with realistic heat fluxes and precise geometry provided by Digital Elevation Models (by using Lidar if possible, or unmanned aerial vehicles in mountainous regions for example), to finally allow truly quantitative parametrization of the model. In this framework, fitting frequent observations during summertime with this thermo-mechanical model allows the acousto-elastic constants to be accurately estimated, and these values can be even better monitored over time. The seasonal fluctuations in acousto-elastic constants may provide new valuable knowledge in terms of erosion processes: if these values increase significantly over a certain time, fracturing and damaging of the material would be suspected. Hence, this new model allows to correct for frequency changes in rock columns caused by environmental (reversible) changes, thus opening the possibility to better detect irreversible frequency drops linked to fracturing, paving the way for better early warning systems to alert to imminent rock column failures.

ACKNOWLEDGMENTS

This work was partially funded by the ANR LABCOM GEO3ILAB, and is part of the LABEX OSUG Habitability. We thank the SIG service of ISTerre (Grenoble, France) for experimental help. EL, PB and LB designed and supported the seismic experiments at the Les Arches site. Data processing, seismic observations and study site description were performed by PB. AG developed the thermo-mechanical modelling and analysed the results, in close collaboration with LB and EL. AG prepared and wrote the manuscript with contributions and reviews from all co-authors.

Data availability statement

The data underlying this paper will be shared on reasonable request to the corresponding author.

Conflict of Interest

The authors declare that they have no conflict of interest.

References

Amaral Vargas, E. do, Velloso, R.Q., Chávez, L.E., Gusmão, L. & Amaral, C.P. do, 2013. On the effect of thermally induced stresses in failures of some rock slopes in Rio de Janeiro, Brazil, *Rock Mech. Rock Eng.,* **46,** 123–134.

Bach, F. & Askegaard, V., 1979. General stress-velocity expressions in acoustoelasticity, *Exper. Mech.,* **19,** 69–75.

Bièvre, G., Franz, M., Larose, E., Carrière, S., Jongmans, D. & Jaboyedoff, M., 2018. Influence of environmental parameters on the seismic velocity changes in a clayey mudflow (Pont-Bourquin Landslide, Switzerland), *Eng. Geol.,* **245,** 248–257.

Bottelin, P. *et al.*, 2017. Monitoring rock reinforcement works with ambient vibrations: La Bourne case study (Vercors, France), *Eng. Geol.,* **226,** 136–145.

Bottelin, P., Lévy, C., Baillet, L., Jongmans, D. & Guéguen, P., 2013. Modal and thermal analysis of Les Arches unstable rock column (Vercors massif, French Alps), *Geophys. J. Int.,* **194,** 849–858.

Bottelin, Pierre, Baillet, L., Carrier, A., Larose, E., Jongmans, D., Brenguier, O. & Cadet, H., 2021. Toward workable and cost-efficient monitoring of unstable rock compartments with ambient noise, *Geosciences,* **11,** 242, doi:10.3390/geosciences11060242

Burjánek, J., Gassner-Stamm, G., Poggi, V., Moore, J.R. & Fäh, D., 2010. Ambient vibration analysis of an unstable mountain slope, *Geophys. J. Int.,* **180,** 820–828.

Burjánek, J., Gischig, V., Moore, J.R. & Fäh, D., 2018. Ambient vibration characterization and monitoring of a rock slope close to collapse, *Geophys. J. Int.,* **212,** 297–310.

Collins, B.D. & Stock, G.M., 2016. Rockfall triggering by cyclic thermal stressing of exfoliation fractures, *Nature Geosci.,* **9,** 395–400.

Collins, B.D., Stock, G.M., Eppes, M.-C., Lewis, S.W., Corbett, S.C. & Smith, J.B., 2018. Thermal influences on spontaneous rock dome exfoliation, *Nat Commun.,* **9,** 762. doi:10.1038/s41467-017-02728-1

Colombero, C., Baillet, L., Comina, C., Jongmans, D., Larose, E., Valentin, J. & Vinciguerra, S., 2018. Integration of ambient seismic noise monitoring, displacement and meteorological measurements to infer the temperature-controlled long-term evolution of a complex prone-to-fall cliff, *Geophys. J. Int.,* **213,** 1876–1897.

Colombero, C. *et al.*, 2015. Spectral analysis and correlation of ambient seismic noise. The case study of Madonna del Sasso (NW Italy),in *Presented at the Near Surface Geoscience 2015 - 21st European Meeting of Environmental and Engineering Geophysics*. doi:10.3997/2214-519 4609.201413666

Colombero, C. *et al.*, 2016. Comparison of microseismic-event and ambient-noise strategies for rock-mass monitoring, pp. 550–552, Presented at the 35° convegno Nazionale GNGTS, Lugliоprint. Retrieved from, https://iris.unito.it/handle/2318/1640267.

Colombero, C., Godio, A. & Jongmans, D., 2021b. Ambient seismic noise and microseismicity monitoring of a prone-to-fall quartzite tower (Ormea, NW Italy), *Remote Sens.,* **13,** 1664, Multidisciplinary Digital Publishing Institute. doi:10.3390/rs13091664

Colombero, C., Jongmans, D., Fiolleau, S., Valentin, J., Baillet, L. & Bièvre, G., 2021a. Seismic noise parameters as indicators of reversible modifications in slope stability: a review, *Surv. Geophys.,* **42,** 339–375.

COMSOL Multiphysics®, 2022. Stockholm, Sweden:, COMSOL A.B., Retrieved from, www.comsol.com.

Dietze, M., Krautblatter, M., Illien, L. & Hovius, N., 2020. Seismic constraints on rock damaging in a failing mountain peak: the Hochvogel, Allgäu (preprint), EarthArXiv. doi:10.31223/osf.io/kz679

Draebing, D., Haberkorn, A., Krautblatter, M., Kenner, R. & Phillips, M., 2017. Thermal and mechanical responses resulting from spatial and temporal snow cover variability in permafrost rock slopes, Steintaelli, Swiss Alps, *Permafrost Periglacial Process.,* **28,** 140–157.

Feng, Z., Qiao, M., Dong, F., Yang, D. & Zhao, P., 2020. Thermal expansion of triaxially stressed mudstone at elevated temperatures up to 400°C, *Adv. Mater. Sci. Eng.,* **2020,** e8140739, Hindawi, doi:10.1155/2020/8140739

Fiolleau, S., Jongmans, D., Bièvre, G., Chambon, G., Baillet, L. & Vial, B., 2020. Seismic characterization of a clay-block rupture in Harmalière landslide, French Western Alps, *Geophys. J. Int.,* **221,** 1777–1788.

Gischig, V.S., Eberhardt, E., Moore, J.R. & Hungr, O., 2015. On the seismic response of deep-seated rock slope instabilities — insights from numerical modeling, *Eng. Geol.,* **193,** 1–18.

Grechi, G., Fiorucci, M., Marmoni, G.M. & Martino, S., 2021. 3D thermal monitoring of jointed rock masses through infrared thermography and photogrammetry, *Remote Sens.,* **13,** 957, Multidisciplinary Digital Publishing Institute. doi:10.3390/rs13050957

Grechi, G. & Martino, S., 2021. *Multimethodological Study of Non-linear Strain Effects Induced by Thermal Stresses on Jointed Rock Masses. in Understanding and Reducing Landslide Disaster Risk: Volume 5 Catastrophic Landslides and Frontiers of Landslide Science ICL Contribution to Landslide Disaster Risk Reduction eds,* Vilímek, V., Wang, F., Strom, A., Sassa, K., Bobrowsky, P.T. & Takara, K., pp. 315–321, Cham: Springer International Publishing.

Guerin, A. *et al.*, 2019. Detection of rock bridges by infrared thermal imaging and modeling. *Sci. Rep.,* **9,** 13138, doi:10.1038/s41598-019-49336-1

Guyer, R.A. & Johnson, P.A., 2009. *Nonlinear Mesoscopic Elasticity: The Complex Behaviour of Rocks, Soil, Concrete,* John Wiley & Sons.

Häusler, M., Michel, C., Burjánek, J. & Fäh, D., 2019. Fracture network imaging on rock slope instabilities using resonance mode analysis, *Geophys. Res. Lett.,* **46,** 6497–6506.

Hughes, D.S. & Kelly, J.L., 1953. Second-order elastic deformation of solids, *Phys. Rev.,* **92,** 1145–1149, American Physical Society.

Iannucci, R., Martino, S., Paciello, A., D'Amico, S. & Galea, P., 2018. Engineering geological zonation of a complex landslide system through seismic ambient noise measurements at the Selmun Promontory (Malta), *Geophys. J. Int.,* **213,** 1146–1161.

Johnson, P., Guyer, R. & Ostrovsky, L., 1999. A nonlinear mesoscopic elastic class of materials (No. LA-UR-99-4733), Los Alamos National Lab, (LANL), Los Alamos, NM (United States). Retrieved from, https://www.osti.gov/biblio/768239.

Larose, E., de Rosny, J., Margerin, L., Anache, D., Gouedard, P., Campillo, M. & Tiggelen, B. van., 2006. Observation of multiple scattering of kHz vibrations in a concrete structure and application to monitoring weak changes, *Phys. Rev. E,* **73,** 016609, American Physical Society. doi:10.1103/PhysRevE.73.016609

Larose, E. *et al.*, 2015. Environmental seismology: what can we learn on earth surface processes with ambient noise?, *J. appl. Geophys.,* **116,** 62–74.

Larose, E. & Hall, S., 2009. Monitoring stress related velocity variation in concrete with a $2\times10-5$ relative resolution using diffuse ultrasound, *J. acoust. Soc. Am.,* **125,** 1853–1856.

Le Breton, M., Larose, É., Baillet, L., Bontemps, N. & Guillemot, A., 2021. Landslide monitoring using seismic ambient noise interferometry: challenges and applications, *Earth-Sci. Rev,* **216,** 103518, doi.org/10.1016/j.earscirev.2021.103518.

Leith, K., Perras, M., Siren, T., Rantanen, T., Heinonen, S. & Loew, S., 2017. Dynamic fracture development in response to extreme summer temperatures: 27/7/2014, Långören Island, Finland, in *Presented at the EGU General Assembly Conference Abstracts,* 19th EGU General Assembly, EGU2017, Vienna, Austria, 16387.

Lévy, C., Baillet, L., Jongmans, D., Mourot, P. & Hantz, D., 2010. Dynamic response of the Chamousset rock column (Western Alps, France), *J. geophys. Res.,* **115,** doi:10.1029/2009JF001606

Levy, C., Jongmans, D. & Baillet, L., 2011. Analysis of seismic signals recorded on a prone-to-fall rock column (Vercors massif, French Alps), *Geophys. J. Int.,* **186,** 296–310.

Lowrie, W. & Fichtner, A., 2020. *Fundamentals of Geophysics,* Cambridge University Press.

Mainsant, G., Larose, E., Brönnimann, C., Jongmans, D., Michoud, C. & Jaboyedoff, M., 2012. Ambient seismic noise monitoring of a clay landslide: toward failure prediction, *J. geophys. Res.,* **117.**

Marmoni, G.M., Fiorucci, M., Grechi, G. & Martino, S., 2020. Modelling of thermo-mechanical effects in a rock quarry wall induced by near-surface temperature fluctuations, *Int. J. Rock Mech. Mining Sci.,* **134,** 104440. doi:10.1029/2011JF002159

Murnaghan, F.D. 1951. *Finite Deformation of an Elastic Solid,* Wiley, New-York.

Planès, T. & Larose, E., 2013. A review of ultrasonic Coda Wave Interferometry in concrete, *Cement Concrete Res.,* **53,** 248–255.

Racek, O., Blahůt, J. & Hartvich, F., 2021a. Observation of the rock slope thermal regime, coupled with crackmeter stability monitoring: initial results from three different sites in Czechia (central Europe), *Geosci. Instrum. Methods Data Syst.,* **10,** 203–218, Copernicus GmbH.

Racek, O., Blahůt, J. & Hartvich, F., 2021b. Monitoring of thermoelastic wave within a rock mass coupling information from IR camera and crack meters: a 24-hour experiment on "Branická Skála" rock in Prague, Czechia. in *Understanding and Reducing Landslide Disaster Risk: Volume 3 Monitoring and Early Warning ICL Contribution to Landslide Disaster Risk Reduction,* Casagli, N., Tofani, V., Sassa, K., Bobrowsky, P.T. & Takara, K., eds, pp. 41–48, Cham: Springer International Publishing.

Richter, T., Sens-Schönfelder, C., Kind, R. & Asch, G., 2014. Comprehensive observation and modeling of earthquake and temperature-related seismic velocity changes in northern Chile with passive image interferometry, *J. geophys. Res.: Solid Earth,* **119,** 4747–4765.

Starr, A.M., Moore, J.R. & Thorne, M.S., 2015. Ambient resonance of Mesa Arch, Canyonlands National Park, Utah, *Geophys. Res. Lett.,* **42,** 6696–6702.

Tsai, V.C. 2011. A model for seasonal changes in GPS positions and seismic wave speeds due to thermoelastic and hydrologic variations, *J. geophys. Res.: Solid Earth,* **116,** doi:10.1029/2010JB008156

Valentin, J. 2018. *Suivi de glissements rocheux et de coulées dans les roches argileuses à partir de méthodes sismiques et photogrammétriques, thesis, Grenoble Alpes,* Retrieved from, http://www.theses.fr/2018GREAU016.

Valentin, J., Capron, A., Jongmans, D., Baillet, L., Bottelin, P., Donze, F., Larose, E. *et al.*, 2017. The dynamic response of prone-to-fall columns to ambient vibrations: comparison between measurements and numerical modelling, *Geophys. J. Int.,* **208,** 1058–1076.

Villarraga, C.J., Gasc-Barbier, M., Vaunat, J. & Darrozes, J., 2018. The effect of thermal cycles on limestone mechanical degradation, *Int. J. Rock Mech. Mining Sci.,* **109,** 115–123.

Vlcko, J., Greif, V., Grof, V., Jezny, M., Petro, L. & Brcek, M., 2009. Rock displacement and thermal expansion study at historic heritage sites in Slovakia, *Environ. Geol.,* **58,** 1727–1740.

Winkler, K.W. & McGowan, L., 2004. Nonlinear acoustoelastic constants of dry and saturated rocks, *J. Geophys. Res.,* **109,** B10204, doi:10.1029/2004JB003262.

Xia, Y., Xu, Y.-L., Wei, Z.-L., Zhu, H.-P. & Zhou, X.-Q., 2011. Variation of structural vibration characteristics versus non-uniform temperature distribution, *Eng. Struct.,* **33,** 146–153.

Xie, F., Ren, Y., Zhou, Y., Larose, E. & Baillet, L., 2018. Monitoring local changes in granite rock under biaxial test: a spatiotemporal imaging application with diffuse waves, *J. geophys. Res.: Solid Earth,* **123,** 2214–2227.

Appendix A: Seismic velocity evolution along rock column cross-section

In this appendix, additional results of the simulation mentioned in the paper are presented (Part 3: Thermo-mechanical model), with both radiative and convective heat fluxes, the maximums of which were synchronized at 4:00 PM.

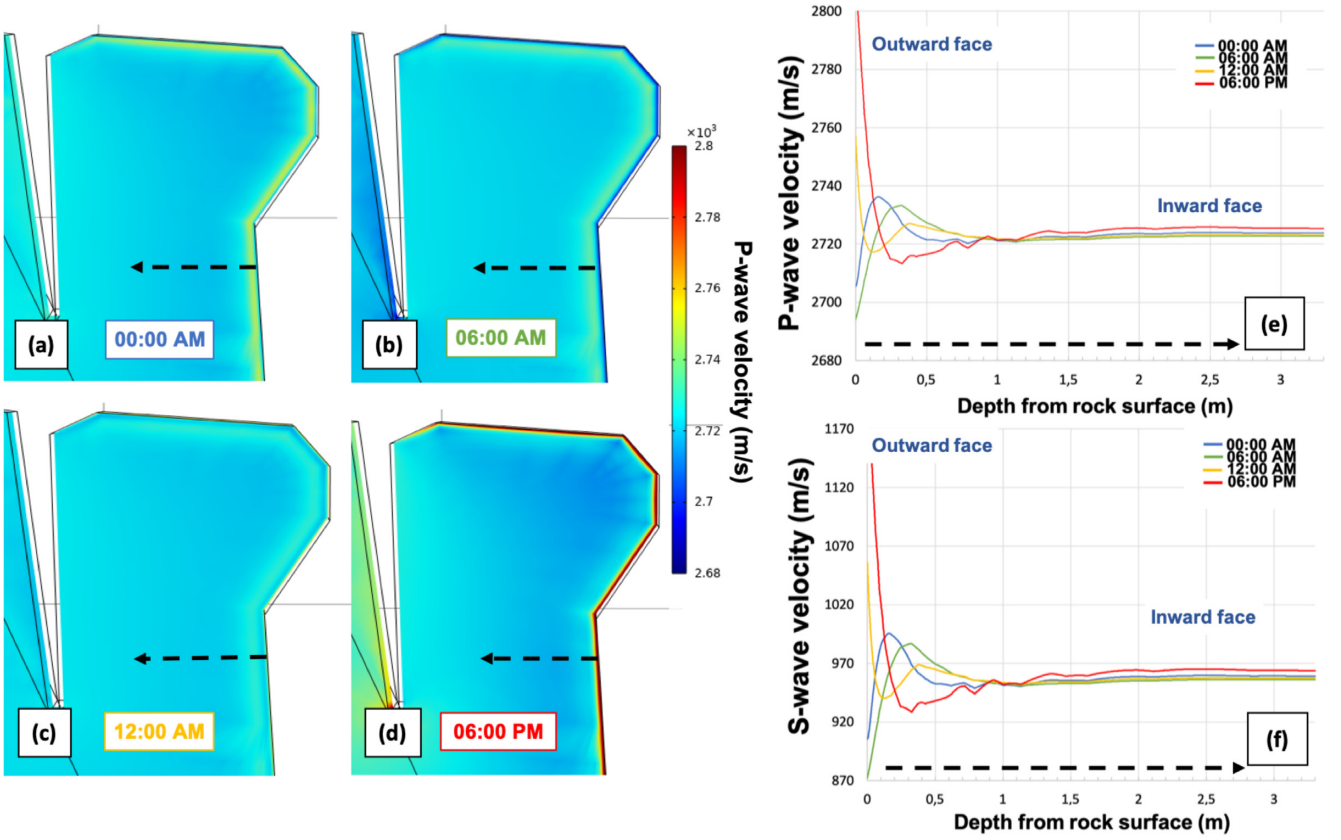

Figure A1. Evolution of the *P*-wave velocity field over time on a vertical cross-section inside the rock model, at scheduled time intervals on day 6 of simulation: midnight (a), 06:00 AM (b), midday (c), and 06:00 PM (d). *P*-wave velocity profiles (e) and *S*-wave velocity profiles (f) along the modelled rock column (highlighted by the dashed black arrow on cross-sections) are also shown at these four times (colour code indicated in the legend).

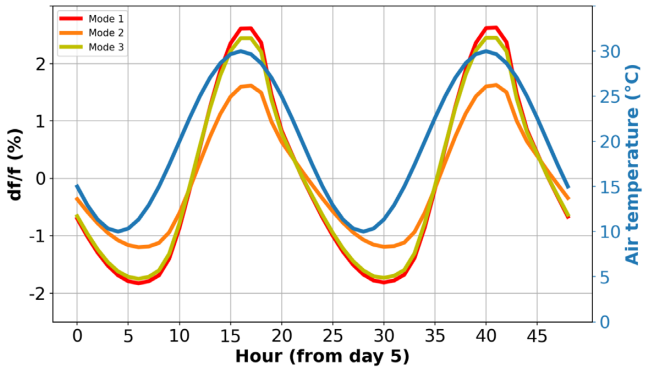

Figure B1. Relative change in resonance frequency of the three first modes of the modelled rock column at Les Arches over time $\Delta f_i / f_i$ (fundamental mode $i = 1$ in red, mode $i = 2$ in orange and mode $i = 3$ in yellow); imposed air temperature T_a is also indicated (in blue). The modelled radiative flux Q_{rad} was shifted two hours earlier than the simulation, for which results are shown in Fig. 5. Only two days at steady state (days 5 and 6) of the transient simulation TTMA are shown.

Appendix B: Influence of thermal flux timing on thermo-mechanical results

Here, the results of the simulation mentioned in the paper are presented (Part 3: Thermo-mechanical modelling), using the same parametrization except the timing of heat fluxes: the convective flux modelled Q_{conv} is kept unchanged (maximum at 4:00 PM), but the modelled radiative flux Q_{rad} is shifted to two hours earlier (maximum at 2:00 PM). The goal of this run was to assess how far our results (frequency variations over time) depend on the timing of heat fluxes, with realistic cases.

Compared to the simulation described in the main part of the paper, the $\Delta f_{1n} / f_{1n}$ amplitude was slightly lower (±2.2 per ecnt versus ±2.3 per cent, see Fig. B1 and Fig. 5) and the $\Delta f_{1n} / f_{1n}$ maximum emerged more than one hour earlier (5:30 PM instead of 6:30 PM). The pattern of fracture opening is also sinusoidal, and fracture closing reaches its maximum at around 5:00 PM (instead of 6:30 PM). The relation between fracture displacement and resonance frequency shows a tiny distortion (Fig. B2d), with frequency delayed by about an hour.

Appendix C: Thermo-mechanical results with only convective forcing

Here, we present the results of the simulation mentioned in the paper (Part 3: Thermo-mechanical modelling), using the same parameters, but only convective heat flux Q_{conv} (no forced radiative flux Q_{rad}). The goal of this run was to quantitatively assess the sensitivity of our results (frequency variations of vibrating modes and fracture displacement) to heat fluxes, and the respective influence of convective and radiative forcing on our results.

Compared to the simulation described in the main part of the paper, the amplitude of $\Delta f_i / f_i$ is much lower (±1.1 per cent compared to ±2.3 per cent, see respectively Fig. C1 and Fig. 5) whereas the timing of the $\Delta f_i / f_i$ maximum is almost unchanged (around 6:30 PM). As well as air temperature and frequencies, the fracture opening pattern shows a sinusoidal pattern over time, and fracture closing reaches its maximum at around 6:30 PM. Fracture displacement and resonance frequency are slightly out of phase (Fig. C2d); with frequency late by a few minutes.

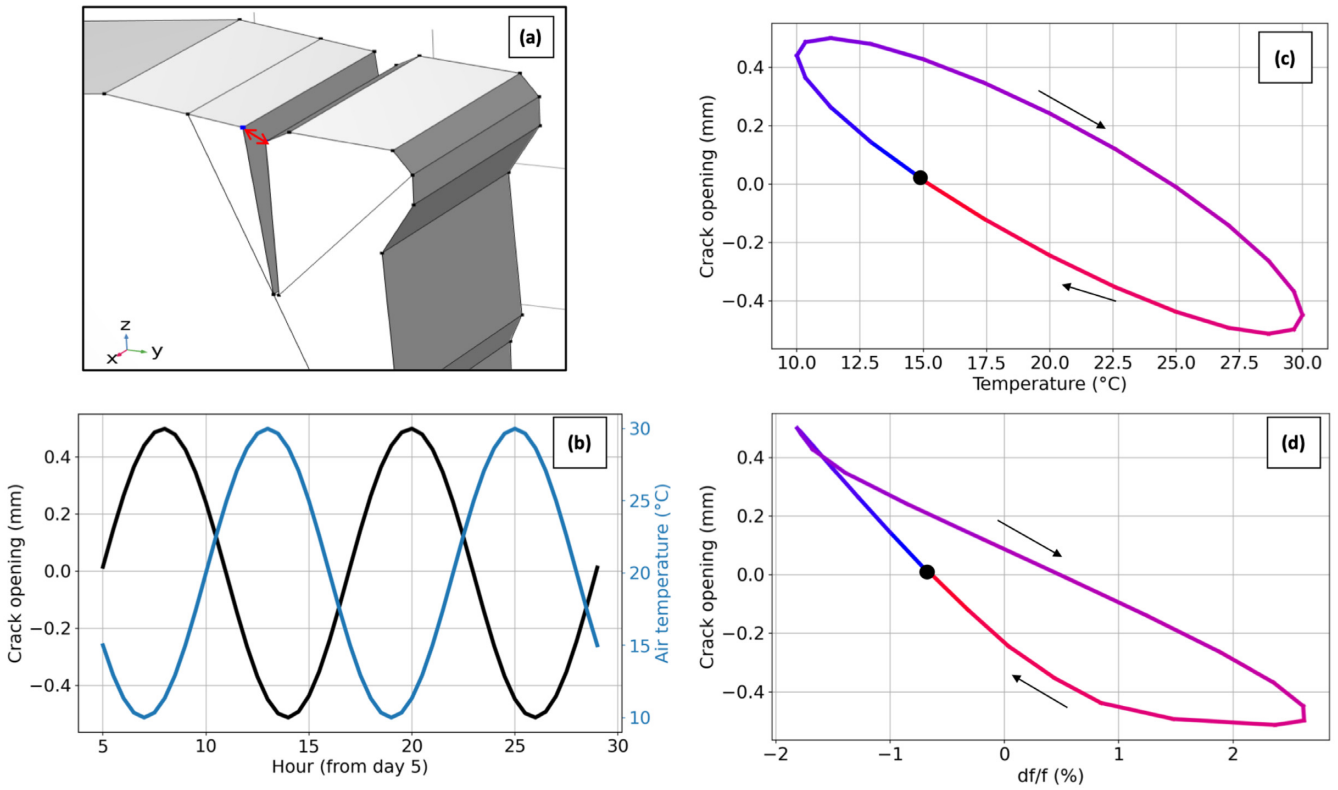

Figure B2. (a) Crack displacement is defined as the gap between the two points on either side of the RF, as indicated by the red arrow. (b) Air temperature T_a (in blue) and crack opening (in black) over two days at steady state. Crack displacement is defined as the gap between the two points on either side of the RF, as depicted above by the red arrow. (c) Changes to crack opening with respect to air temperature T_a, over one day at steady state. (d) Changes to crack opening with respect to the relative variation in fundamental resonance frequency f_{1n}, over one day at steady state. For (c) and (d), time is indicated by the line colour, from blue at the beginning (00:00 AM) to red at the end of the day (11:59 PM). For this simulation, the modelled radiative flux was shifted two hours earlier than the simulation for which results are show in Fig. 7.

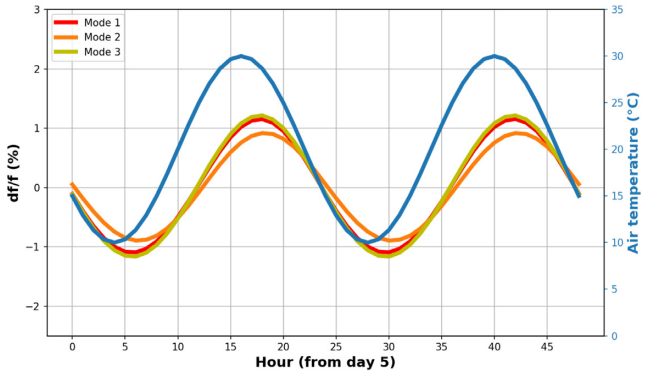

Figure C1. Relative change in resonance frequency of the three first modes of the modelled rock column Les Arches $\Delta f_i / f_i$ over time (fundamental mode $i = 1$ in red, mode $i = 2$ in orange and mode $i = 3$ in yellow), along with imposed air temperature T_a (in blue). Only convective heat flux Q_{conv} was applied in this simulation, in contrast to the simulation shown in Fig. 5. Only two days at steady state (days 5 and 6) of the transient simulation TTMA are shown.

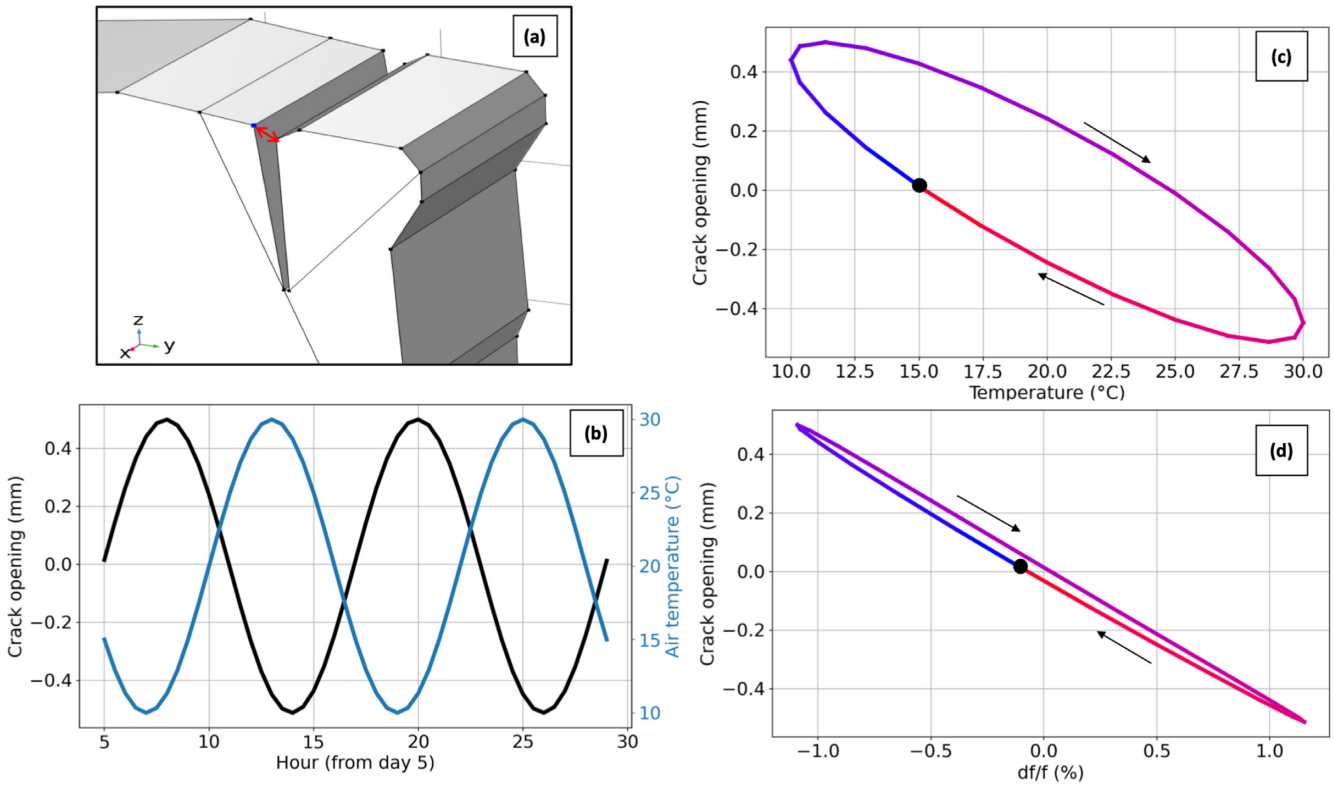

Figure C2. (a) Crack displacement is defined as the gap between the two points on either side of the RF, as indicated by the red arrow. (b) Air temperature T_a (in blue) and crack opening (in black) over time for two days at steady state. Crack displacement is defined as the gap between the two points on either side of the RF, as depicted above by the red arrow. (c) Changes in crack opening with respect to the air temperature T_a, over one day at steady state. (d) Changes in crack opening with respect to the relative variation of fundamental resonance frequency f_{1n}, over one day at steady state. For (c) and (d), time is indicated by the line colour, from blue at the beginning (00:00 AM) to red at the end of the day (11:59 PM). Only convective heat flux Q_{conv} was applied for this simulation, in contrast to the simulation shown in Fig. 7.